

# Attosecond probing and control of charge migration in carbon-chain molecule

Lixin He,<sup>a</sup> Yanqing He,<sup>a</sup> Siqi Sun,<sup>a</sup> Esteban Goetz,<sup>b</sup> Anh-Thu Le,<sup>b</sup> Xiaosong Zhu,<sup>a</sup> Pengfei Lan,<sup>a,\*</sup> Peixiang Lu,<sup>a,c,\*</sup> and Chii-Dong Lin<sup>d</sup>

<sup>a</sup>Huazhong University of Science and Technology, Wuhan National Laboratory for Optoelectronics and School of Physics, Wuhan, China

<sup>b</sup>University of Connecticut, Department of Physics, Storrs, Connecticut, United States

<sup>c</sup>Wuhan Institute of Technology, Hubei Key Laboratory of Optical Information and Pattern Recognition, Wuhan, China

<sup>d</sup>Kansas State University, Department of Physics, Manhattan, Kansas, United States

**Abstract.** In quantum mechanics, when an electron is quickly ripped off from a molecule, a superposition of new eigenstates of the cation creates an electron wave packet that governs the charge flow inside, which has been called charge migration (CM). Experimentally, extracting such dynamics at its natural (attosecond) timescale is quite difficult. We report the first such experiment in a linear carbon-chain molecule, butadiyne ( $C_4H_2$ ), via high-harmonic spectroscopy (HHS). By employing advanced theoretical and computational tools, we showed that the wave packet and the CM of a single molecule are reconstructed from the harmonic spectra for each fixed-in-space angle of the molecule. For this one-dimensional molecule, we calculate the center of charge  $\langle x \rangle(t)$  to obtain  $v_{cm}$ , to quantify the migration speed and how it depends on the orientation angle. The findings also uncover how the electron dynamics at the first few tens to hundreds of attoseconds depends on molecular structure. The method can be extended to other molecules where the HHS technique can be employed.

Keywords: attosecond charge migration; high-harmonic spectroscopy; single-molecule harmonic dipole; machine learning.

Received Apr. 26, 2023; revised manuscript received Jun. 25, 2023; accepted for publication Jul. 27, 2023; published online Aug. 24, 2023.

© The Authors. Published by SPIE and CLP under a Creative Commons Attribution 4.0 International License. Distribution or reproduction of this work in whole or in part requires full attribution of the original publication, including its DOI.

[DOI: [10.1117/1.AP.5.5.056001](https://doi.org/10.1117/1.AP.5.5.056001)]

## 1 Introduction

Ultrafast electron dynamics are of crucial importance for understanding and steering complex chemical and biological reactions. When subjected to an intense laser field, a pure electron-driven dynamic can be initiated by strong field ionization of the molecule. Theoretically, this dynamic manifests itself as a migration of the initially created hole density through the molecular backbone and was dubbed charge migration (CM) in 1999.<sup>1</sup> In the last decade, CM has been extensively studied theoretically using time-dependent quantum chemistry packages.<sup>2–13</sup> Topics of interest include the dependence of CM on molecular species and structures,<sup>9–13</sup> as well as the role of nuclear dynamics and decoherence in CM.<sup>14–16</sup> In these numerical studies, calculations were made to follow the time evolution of the density of

the wave packet under the field-free condition. However, these results cannot be tested against experiments directly. In a real experiment, to know the field-free wave packet (or CM), a probe pulse is needed, which will inevitably affect the evolution of the wave packet. Thus, retrieving the field-free CM from the measurement is a monumental task and rarely possible.

Since it is a fascinating goal of ultrafast science to follow electron and/or nuclear dynamics, in spite of the difficulty, it is still desirable to perform pump–probe experiments to extract some partial information. For CM in molecules, it occurs at a timescale of a few tens of attoseconds. Then one would like to have pump and probe pulses shorter than a few femtoseconds. Such pulses, however, would have a bandwidth of a few tens of electron volts, and the created wave packet would be very complicated for studying valence electrons in a molecule. Additionally, the currently available attosecond pulses are still not intense enough for such applications. To date, most electron dynamics studies have used attosecond pump and intense IR

\*Address all correspondence to Pengfei Lan, [pengfeilan@hust.edu.cn](mailto:pengfeilan@hust.edu.cn); Peixiang Lu, [lupeixiang@hust.edu.cn](mailto:lupeixiang@hust.edu.cn)

probe pulses, or vice versa.<sup>17–21</sup> Among the experiments that studied electron dynamics or CM, most of them are unable to obtain electron wave packets or the dynamics of CM for individual molecules directly.

From strong-field physics, it has long been suggested that one can use high-harmonic spectroscopy (HHS) to study attosecond electron dynamics using intense infrared lasers (see the reviews<sup>22,23</sup>). The principle of HHS is based on the three-step process of high-order harmonic generation (HHG),<sup>24,25</sup> where an electron is first ionized near the peak of the laser field, the released electron then drifts in the laser field, and some portion will be driven back to recombine with the ion and emit harmonic radiation. At the time of recombination, the information of the electron wave packet of the cation is encoded in both the amplitude and phase of each generated harmonic. The intrinsic time-to-frequency mapping underlying HHG allows a temporal measurement of the electron dynamics with a resolution of tens to a hundred attoseconds.<sup>26–32</sup> Up to now, HHS has been well used for ultrafast molecular detection including static molecular orbital tomography<sup>33–35</sup> and also dynamic imaging of nuclear and electron motions.<sup>26–32</sup>

Although the HHS principle is easy to understand, implementing it for extracting accurate CM for each single molecule is not so straightforward, since the experimentally measured harmonic spectra are due to the coherent summation of the individual radiation weighted by the angular distribution of the molecules. In the first experiment of using HHS to extract the CM by Kraus et al.,<sup>26</sup> the measured angularly integrated harmonic spectra were directly taken as the single-molecule results. In doing so, large errors are introduced into the reconstructed dynamics. In our recent paper,<sup>36</sup> we developed a machine-learning (ML) algorithm to retrieve the single-molecule harmonics from the angularly integrated harmonic spectra, opening an avenue for accurate measurement of CM on the single-molecule level.

In spite of that, the sensitive dependence of CM on molecular orbitals and orientations still makes the CM dynamics complex and difficult to trace. There are still some open questions about CM that remain unclear; for example, how fast does the charge migrate in molecules? Very recently, by creating a localized wave packet, the hole has been predicted to migrate along the molecular backbone in a particle-like manner at a speed of a few Å/fs.<sup>10</sup> However, in most reactions involving valence electrons, delocalized wave packets are created. In addition, the electron wave packet cannot be measured directly. They have to be reconstructed from other experimental data. In this work, we focus on a linear carbon chain molecule, butadiyne ( $C_4H_2$ ), where the movement of the hole is expected to be along the carbon backbone.<sup>9</sup> Using an ML algorithm to analyze the harmonic spectra measured from aligned  $C_4H_2$  in a two-color driving field, we successfully retrieved the hole wave packet of the cation in  $C_4H_2^+$ . From the center of charge (COC) at each time, the CM speed was measured for the first time. Our approach allows us to extract how migration speed depends on the alignment angle of the molecule, whether the charge density is localized<sup>10–12</sup> or delocalized.

## 2 Results and Discussion

Figure 1 sketches the multichannel mechanism of HHG from the  $C_4H_2$  molecule. Exposed to an intense external laser field, the ground  $\tilde{X}^2\Pi_g$  ( $\tilde{X}$ ) and the first excited  $\tilde{A}^2\Pi_u$  ( $\tilde{A}$ ) states of the  $C_4H_2^+$  ion, which correspond to the removal of an electron from the highest and second-highest occupied molecular orbitals HOMO and HOMO-1, respectively, can be simultaneously

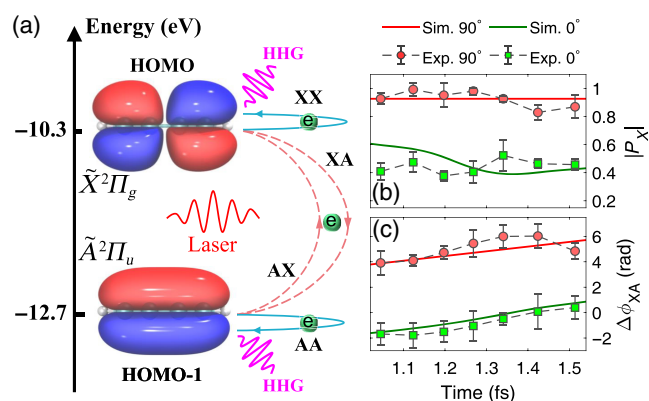


**Fig. 1** Probing CM in  $C_4H_2$  with HHS. (a) Schematic layout of the multichannel HHG in  $C_4H_2$  molecule that involves the ground  $\tilde{X}^2\Pi_g$  ( $\tilde{X}$ ) and first excited states  $\tilde{A}^2\Pi_u$  ( $\tilde{A}$ ) of the molecular ion. In  $C_4H_2$ , there are four channels labeled as XX, AA, XA, and AX, respectively, contributing to HHG. Here the first and second letters label the ionic state after ionization and before recombination, respectively. (b), (c) Experimentally retrieved population amplitude ( $|P_X|$ ) of the  $\tilde{X}$  state (b) and the relative phase ( $\Delta\phi_{XA}$ ) between the wave functions of  $\tilde{X}$  and  $\tilde{A}$  states (c) for the parallel (0 deg, green squares) and perpendicular (90 deg, red circles) alignment of the  $C_4H_2$  molecule. The solid lines show the TDDFT results for comparison. Error bars in panels (b) and (c) represent the SDs of the reconstructions, which are estimated from the experimental errors of the HHG signals with the bootstrap method.

populated by the strong-field ionization due to their close vertical ionization potentials ( $\Delta E = 2.4$  eV). The coherent superposition of multiple electronic states of the molecular ion creates a many-electron wave packet, which evolves in time, leading to the time-dependent variation of the charge density, i.e., the CM in the molecular ion. In the HHG process, these ionic states act as the intermediate that connects the same initial and final state of the system. The presence of different ionic states between the ionization and recombination provides different channels for the harmonic radiation.<sup>37–39</sup> For  $C_4H_2$ , it includes two diagonal channels XX, AA, and two off-diagonal channels XA and AX, as shown in Fig. 1(a). The off-diagonal channels reflect the laser-induced coupling between the two ionic states during the HHG process. Eventual harmonic radiation is a coherent superposition of each channel,<sup>37–39</sup> i.e.,

$$D(\omega, \theta) = \sum_{i,j=X,A} C_{ij}(\theta) d_{ij}(\omega, \theta), \quad (1)$$

where  $D(\omega, \theta)$  is the total dipole moment for HHG, and  $d_{ij}(\omega, \theta)$  is the dipole related to each channel, which in our reconstruction is calculated by the quantitative rescattering theory.<sup>40–43</sup>  $C_{ij}(\theta)$  is a complex mixing coefficient related to the laser-induced transitions between the two ionic states during the harmonic generation process. Equation (1) suggests that the electron dynamics is naturally recorded in the harmonic spectrum and can be deciphered by disentangling the multichannel contributions from the total dipole moment.

In this work, we have carried out HHG experiment of  $C_4H_2$  using a commercial Ti:sapphire laser system (Astrella-USP-1K, Coherent, Inc.), which delivers 35 fs, 800 nm laser pulses at a

repetition rate of 1 kHz. The output laser is split into two beams. One, with moderate intensity (aligning pulse) is used to create nonadiabatic alignment of  $C_4H_2$  molecule. The other intense one (probe pulse) is used to generate high-order harmonics. The aligning and probe pulses are parallel in the polarization (for more experimental details, see [Supplementary Material](#)). In our experiment, we first measured the HHG from  $C_4H_2$  molecule with a one-color driving scheme. The measured HHG signals at different time delays between the probe and aligning pulses were used to determine the alignment distribution in our experiment with the method reported in Ref. 44. With molecular alignment distribution determined, the ML algorithm developed in Ref. 36 then was used to analyze the delay-dependent HHG data to disentangle the coherent angular average of high harmonics originating from the imperfect molecular alignment in experiment, since this angular average could compromise the measurement from the real single-molecule response.<sup>45–47</sup> This is especially important for a low degree of molecular alignment in our experiment, which has  $\langle \cos^2 \theta \rangle \approx 0.5$  (see Fig. S2 in the [Supplementary Material](#)).

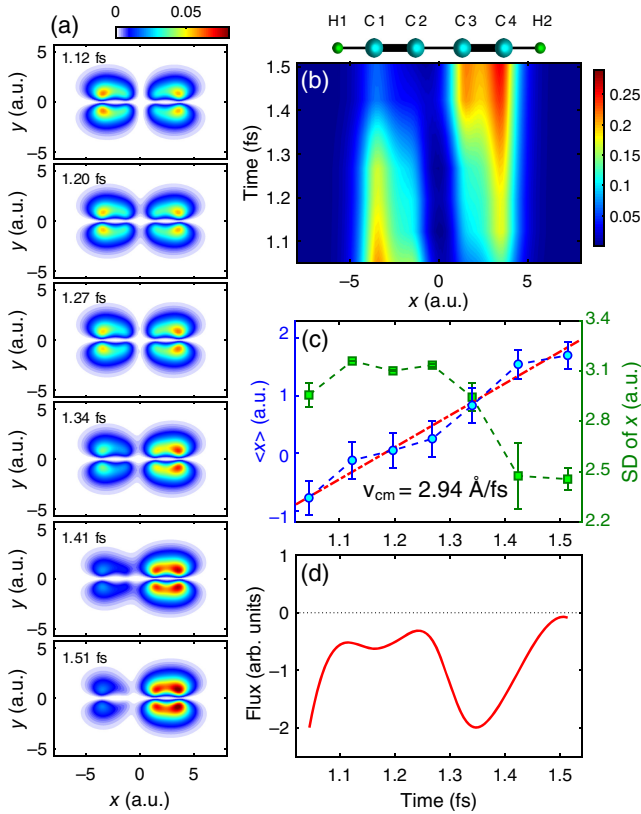
Second, to extract the CM dynamics, multiple experimental observables are required to decompose the multichannel contributions, since in the one-color laser field, only one set of  $D(\omega, \theta)$  can be obtained for each harmonic order, which is insufficient for the decomposition. Here we introduce a two-color driving scheme, where the laser field is synthesized by an intense 800 nm fundamental field and a weak second-harmonic (SH) field that has the same polarization direction as the fundamental one (for experimental details, see [Supplementary Material](#)) to generate high-order harmonics. In our experiment, the SH field used is weak ( $\sim 2 \times 10^{-3}$  of the fundamental field), which barely alters the electron dynamics of the molecular ion (see [Supplementary Material](#)), but could affect the harmonic radiation of each channel. The measurements at different relative phases of the two-color fields thus can replenish the data set required for the reconstruction. By applying the ML-based reconstruction procedure<sup>36</sup> to the measurements at different two-color relative phases, we are able to obtain the complex mixing coefficients of the multiple orbitals of the molecular cation, for each fixed-in-space angle, at the instant of recombination when each harmonic order occurs. To ensure the one-to-one mapping between the instant time and harmonic order, the short electron trajectory has been selected by phase matching in the experiment.

Figure 1(b) shows the time-dependent population amplitudes of the ground state  $\tilde{X}$  ( $|P_X\rangle$ ) of  $C_4H_2^+$  ion extracted from the experimental data of H11 to H17 (including both even and odd orders) for the molecules aligned at 0 deg (squares) and at 90 deg (circles) to the polarization of the driving field, respectively. Figure 1(c) displays the corresponding relative phases between the population coefficients of the  $\tilde{X}$  and  $\tilde{A}$  states ( $\Delta\phi_{XA}$ ). In our reconstruction, the uncertainties of the retrieved parameters [error bars in Figs. 1(b) and 1(c)] were estimated from the experimental errors of the HHG signals with the bootstrap method.<sup>48</sup> For comparison, we have simulated the above parameters based on the time-dependent density functional theory (TDDFT). In the TDDFT framework, the molecular system is described by a series of one-particle Kohn–Sham (KS) orbitals, in which the evolution can be obtained by solving the time-dependent Kohn–Sham (TDKS) equations.<sup>49,50</sup> The inclusion of laser-induced coupling between different orbitals in the TDKS equations allows us to simulate the evolution of different

orbitals during the driving laser field. In our calculations, the TDKS equations are solved using the Octopus package<sup>51</sup> with an local-density approximation (LDA) exchange-correlation functional<sup>52</sup> and an average-density self-interaction correction.<sup>53</sup> In our calculations, the molecule is assumed to align along the  $x$  direction. The driving laser field is polarized in the  $x$ – $y$  plane and propagates along the  $z$  direction. The TDKS equations are solved on a Cartesian grid with the size of  $-58.9 \leq x, y, z \leq 58.9$  a.u. The time step in the simulations is fixed at 0.05 a.u., and the spatial spacing is 0.38 a.u. To eliminate artificial reflections from boundaries, the wave function has been multiplied by a  $\sin^{1/6}$ -masking function at each time step. With the time-dependent TDKS orbitals obtained, the transition amplitude  $C_{ij}$  can be calculated by  $C_{ij} = \langle \Psi_j(r, 0) | \Psi_i(r, t) \rangle$ , where  $\Psi_j(r, 0)$  is the initial KS orbital and the subscript denotes the  $\tilde{X}$  and  $\tilde{A}$  states involved in the CM dynamics. As shown in Figs. 1(b) and 1(c), the TDDFT results (solid lines) agree well with the experimental reconstructions.

With the retrieved parameters in Figs. 1(b) and 1(c), we can reconstruct the hole wave packet of the  $C_4H_2^+$  ion. We first examine the results for the 90 deg alignment of the molecules. In this case, by symmetry, the two states are not coupled by the laser, such that populations of the  $\tilde{X}$  and  $\tilde{A}$  states do not change with time; see the red line in Fig. 1(b). In this situation, the reconstructed charge density does change with time, as can be seen in Fig. 2(a), which displays the reconstructed hole densities in  $C_4H_2^+$  ion at the recombination times of H12 to H17. These figures also show substantial hole migration along the molecular backbone ( $x$  axis). Moreover, the hole densities are always symmetric about the  $y = 0$  plane because of the symmetries of the HOMO and HOMO-1 orbitals of  $C_4H_2$ . Note that these results are similar to the field-free CM defined by Cederbaum and Zobeley.<sup>1</sup>

To provide simpler information from the charge density distribution, we extracted the reduced hole density  $\rho_x(t)$  by integrating the hole density over the  $y$  direction. As shown in Fig. 2(b), the hole created by ionization is initially localized at the left  $C_1 \equiv C_2$  triple bond, then spreads over the molecule, and finally is distributed around the right  $C_3 \equiv C_4$  triple bond after about 500 as. To quantify the CM dynamics, we further define the expectation value of the abscissa  $x$  (carbon chain) as the COC position. As shown in Fig. 2(c), the extracted COC position (blue circles) increases almost linearly with time, indicating a unidirectional migration of the hole from the  $-x$  side to the  $+x$  side. By a linear fitting of  $\langle x \rangle(t)$  [the dashed-dotted line in Fig. 2(c)], we can then evaluate the CM speed from the slope, which is about 2.94 Å/fs. This result is close to the theoretical predictions in halogenated hydrocarbon chains.<sup>10</sup> We have also calculated the standard deviation (SD) of the abscissa  $x$  to quantify the degree of localization of the hole during the evolution. As shown in Fig. 2(c), the SD of  $x$  (green squares) increases in the first 200 as and turns to decrease in the last 300 as, which reflects a delocalization-to-localization behavior of the created hole wave packet. The decrease is due to the wave packet beginning to bounce back from the right  $C \equiv C$  bond. At a longer time, the hole was predicted to travel back and forth between the  $C \equiv C$  triple bonds on both sides.<sup>9,10</sup> Such a periodic behavior cannot be fully visualized from the reconstructions in Figs. 2(b) and 2(c) due to the limited temporal window in our measurement. With the retrieved CM speed, we can estimate the CM-mode period or frequency that is critical for describing the periodic dynamics, by



**Fig. 2** Reconstruction of CM in  $C_4H_2^+$  for perpendicular alignment. (a) Snapshots of the reconstructed hole densities for the alignment angle of 90 deg. (b) Time-dependent hole densities along the molecular backbone obtained by integration over the  $y$  direction. For clarity, the molecular backbone has been plotted on the top of panel (b). (c) Time-dependent COC position  $\langle x \rangle(t)$  (dashed line with circles) retrieved from the hole densities in (b). Here the dashed-dotted line is a linear fitting of  $\langle x \rangle(t)$  to evaluate the CM speed, and the green squares represent the SD of the  $x$  coordinate. (d) Flux of charge density crossing the  $x = 0$  plane. Negative value means CM from  $-x$  side to  $+x$  side.

$T_{cm} = 2\pi/\omega_{cm} = 2d_{cm}/v_{cm}$ , where  $d_{cm} = 4.88$  a.u. is the distance between the centers of the two  $C \equiv C$  triple bonds in  $C_4H_2$ , which is approximately the CM distance in  $C_4H_2^+$ . For the quasi-field-free CM, the CM-mode period and frequency are estimated to be 1.76 fs and 2.35 eV, which are close to the results 1.72 fs and 2.4 eV defined by the energy difference between the two ionic states of  $C_4H_2^+$ .

Rigorously, single-hole dynamics are to be obtained with quantum mechanics. From the retrieved complex wave packet, real values of probability density  $\rho_e$  and current density  $\mathbf{J}$  can be obtained, and they have been found to satisfy the equation of continuity,  $\frac{\partial \rho_e}{\partial t} + \nabla \cdot \mathbf{J} = 0$ . In Fig. 2(d), we show the time-dependent total flux crossing the  $x = 0$  plane calculated from the retrieved complex hole wave packet. One can see that the total flux is always negative over the 500 as duration, indicating continuous migration of the charge from  $-x$  side to the  $+x$  side. A near-zero flux near 1.5 fs also reflects that the hole has moved to the right terminal  $C \equiv C$  bond. These results are consistent with the analysis in Fig. 2(c). On the other hand, the flux changes rapidly with time, indicating that the constant speed in Fig. 2(c) is valid only for the speed of the COC. From the

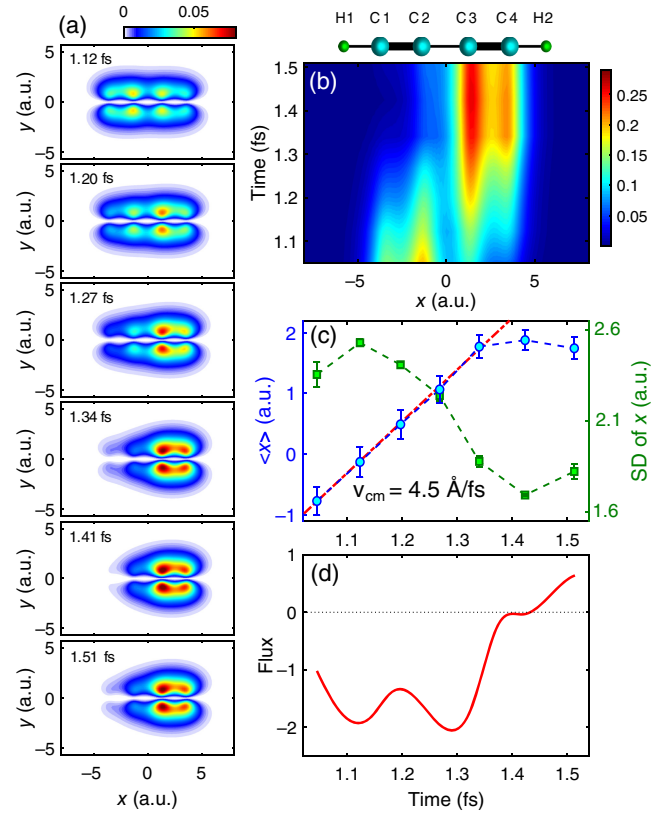


**Fig. 3** Reconstruction of CM in  $C_4H_2^+$  for parallel alignment. (a)–(d) The same as Fig. 2(a)–2(d), but for the case of parallel alignment of the  $C_4H_2$  molecule.

other viewpoint, this would imply that  $v_{cm}$  itself, or the hole density alone, would not provide adequate information on electron dynamics except from the retrieved wave packet. Like electrons and holes in solids,  $v_{cm}$  could provide a first-order interpretation of carrier dynamics, even though the carriers are not localized. This is how the speed of CM is to be understood. It is a measure of how the average position moves.

Proceeding further, next, we consider in Fig. 3 the reconstructed results for the parallel alignment of the molecule. In this case, the ground  $\tilde{X}$  and first excited  $\tilde{A}$  states of  $C_4H_2^+$  are strongly coupled by the laser field due to the large transition dipole moment between these two states along this direction. The resulting CM is controlled by the laser field. Comparing Fig. 2 with Fig. 3, we can see that laser coupling would drive the hole density to  $+x$  side faster [Fig. 3(a)], as well as for the reduced hole density [Fig. 3(b)]. The COC position also rises faster, from which the CM speed has increased to 4.5 Å/fs, even though the SD remains roughly the same, except the feature changes at earlier times [Fig. 3(c)]. Note that here the CM speed is obtained by fitting the COC position  $\langle x \rangle(t)$  before 1.34 fs, where  $\langle x \rangle(t)$  increases almost linearly. Afterward, the hole reaches and localizes at the right terminal  $C \equiv C$  bond. In Fig. 3(d), the flux also shows faster changes with time, indicating that laser coupling has substantially changed the hole density distribution.

To evaluate the reconstructed hole dynamics, we have further performed TDDFT simulations. Figures 4(a) and 4(b) show the time-dependent hole density  $\rho_x(t)$  and the COC position  $\langle x \rangle(t)$  simulated in the same temporal range as in the experiment

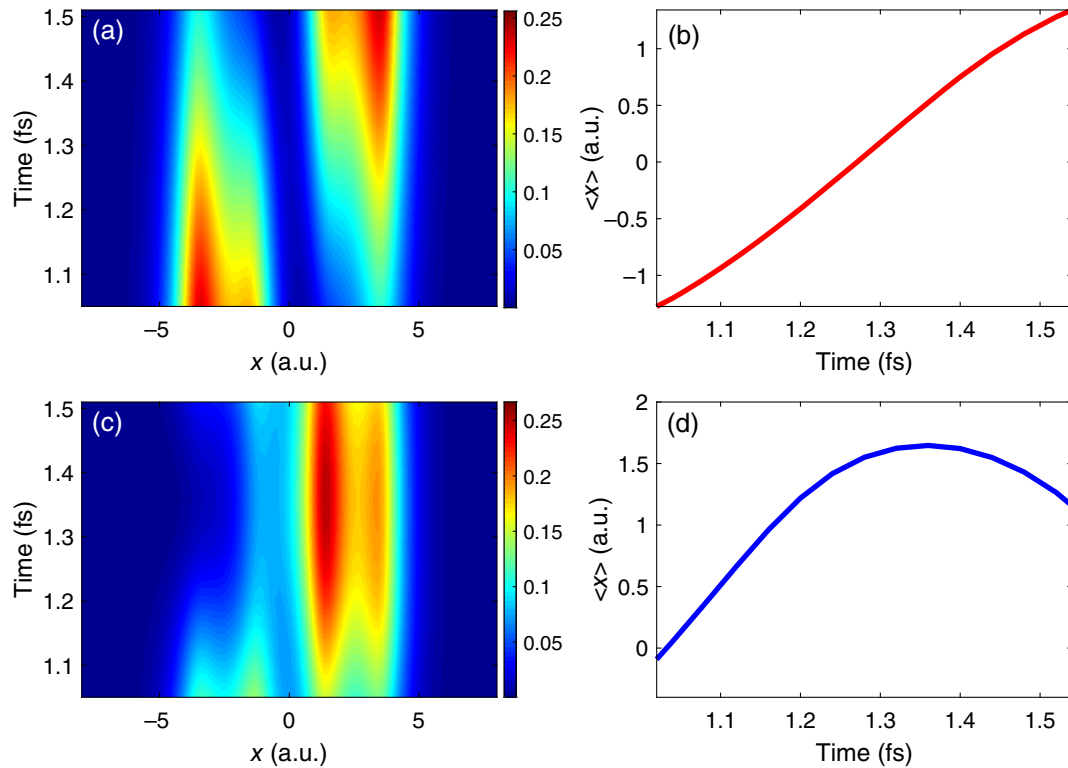


**Fig. 4** TDDFT simulations of the CM dynamics in  $C_4H_2^+$ . (a), (b) TDDFT calculations of the reduced hole density  $\rho_x(t)$  and COC position  $\langle x \rangle(t)$  in the experimental temporal range for the 90 deg alignment of the  $C_4H_2$  molecule. (c), (d) Same as panels (a) and (b), but for the parallel alignment (the alignment angle of 0 deg) of the  $C_4H_2$  molecule.

(i.e., 1.04 to 1.51 fs) for 90 deg alignment of the molecule. One can see that the TDDFT results in Figs. 4(a) and 4(b) agree well with the experimental reconstructions presented in Figs. 2(b) and 2(c). The laser-controlled CM in the parallel aligned molecules has also been simulated. As shown in Figs. 4(c) and 4(d), under the influence of the laser field, the simulated CM dynamics are far different from the field-free result in Figs. 4(a) and 4(b). The simulated  $\langle x \rangle(t)$  increases almost linearly before 1.34 fs and turns to decrease afterward. These results are also in reasonable agreement with the experimental reconstructions in Figs. 3(b) and 3(c).

Using our retrieval method, we are able to obtain CM for all alignment angles at the same time. The CMs for other alignment angles of the fixed-in-space molecules have also been reconstructed (see Figs. S6 and S7 in the [Supplementary Material](#)). The CM speed retrieved as a function of the alignment angles is shown in Fig. 5 (squares). For comparison, the TDDFT results are also presented (solid line). The CM is demonstrated to depend sensitively on the alignment angles. Moreover, the speed of the laser-controlled CM (the cases of non-perpendicular alignments) is faster than the field-free result at 90 deg. The increase of the CM speed mainly arises from the laser-induced coupling between these two cation states. For the 90 deg alignment (field-free case), the timescale of the charge oscillations is determined by the intrinsic energy gap between the two cationic states. While for the 0 deg alignment (and other angles), laser-induced coupling between these two cation states gives rise to a much faster increase in the relative phase between these two states (see Fig. S9 in the [Supplementary Material](#)), which is

equivalent to a larger energy gap between the two cationic states, thus yielding a much faster charge oscillation. This is similar to the well-known fact that the field-free two-level oscillation is slower than the Rabi oscillation when the two levels are driven by an intense laser pulse. In addition, it has been reported that the deviation of the experimentally extracted optimal two-color relative phases  $\varphi_{\max}$ , where the HHG intensity reaches a maximum with respect to the single-active electron

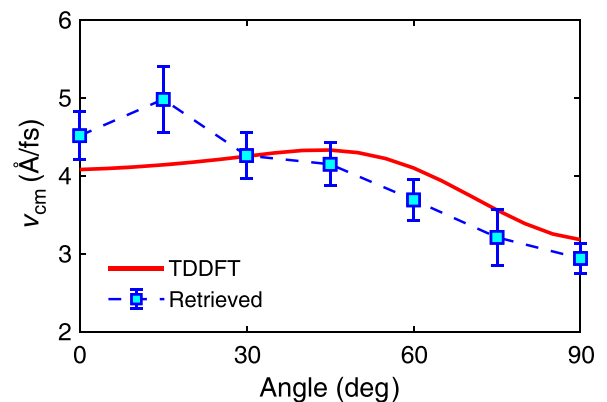


**Fig. 5** Reconstruction of the CM speed in  $C_4H_2^+$ . Dashed line with squares shows the CM speed retrieved as a function of the alignment angles. The solid line plots the TDDFT result for comparison.

response will be a key indicator for the multichannel (CM) dynamics in the molecules.<sup>54</sup> We have examined our two-color measurements and compared them to the single XX channel calculations. The results obtained at the alignment and anti-alignment of C<sub>4</sub>H<sub>2</sub> molecule are shown in Fig. S10 in the [Supplementary Material](#). One can see a clear difference in the deviations of  $\varphi_{\max}$  in the two cases, which provides direct experimental evidence of the different CM dynamics along these two orientations. The alignment dependence of the CM dynamics proves that one should not obtain the corresponding single-molecule dynamics directly from the experiment without angular deconvolution. On the other hand, it also provides a potential way to control the CM speed and even ultimately to manipulate the rate of a chemical reaction.

Finally, it is worth mentioning that in our study of C<sub>4</sub>H<sub>2</sub>, there are only two cationic states involved in the CM dynamics. For other molecules, such as CO<sub>2</sub> molecules,<sup>27,28</sup> more cationic states will participate in the electronic wave packet. In such cases, one can anticipate more complex migration dynamics in the molecule. Due to the different symmetries of the cationic states, the resulting movement of the hole may no longer be solely along the molecular backbone. Instead, the hole could traverse across the molecular backbone or exhibit swirling motion around the constituent atoms.<sup>27,28</sup> In such scenarios, a vertical component of the CM speed (along the *y* direction) should be defined to comprehensively describe the complex migration dynamics in space.

### 3 Conclusions

In summary, CM in a carbon-chain molecule C<sub>4</sub>H<sub>2</sub> was measured using an ML-based two-color HHS method. The CM dynamics are reconstructed at the most fundamental level for each single fixed-in-space molecule. By analyzing the time-dependent hole densities, the speed of CM was extracted for the first time for each alignment angle of the molecule. The retrieval results demonstrate that the laser-controlled CM is much faster than the field-free one. These results are consistent with the TDDFT simulations. Our result provides a simple and intuitive way to understand and quantify the complex CM in molecules. Looking ahead, the method presented here may be extended to driving lasers with much longer wavelengths, in which the whole periodic hole migration may be directly observed from the measurement. On the other hand, oriented halogen-functionalized carbon-chain molecules are also ideal candidates for CM studies in experiments, where the influence of the hole localization on the CM speed may be examined. Moreover, the halogen functionalization can provide another degree of freedom to control the CM.

### Data and Materials Availability

All the data that support the findings of this study are available from the corresponding authors upon reasonable request.

### Acknowledgments

This work was supported by the National Key Research and Development Program of China (No. 2019YFA0308300), the National Natural Science Foundation of China (Nos. 91950202, 12225406, 12074136, 12021004, and 11934006), and the Natural Science Foundation of Hubei Province (No. 2021CFB330). Chii-Dong Lin was supported by the Chemical Sciences, Geosciences, and Biosciences

Division, Office of Basic Energy Sciences, Office of Science, U.S. Department of Energy (No. DE-FG02-86ER13491). Work by E. Goetz and A.T. Le was supported by the U.S. Department of Energy, Office of Science, Office of Basic Energy Sciences (No. DE-SC0023192). The authors declare no conflicts of interest.

### References

1. L. S. Cederbaum and J. Zobeley, "Ultrafast charge migration by electron correlation," *Chem. Phys. Lett.* **307**, 205–210 (1999).
2. A. I. Kuleff, J. Breidbach, and L. S. Cederbaum, "Multielectron wave-packet propagation: general theory and application," *J. Chem. Phys.* **123**, 044111 (2005).
3. J. Breidbach and L. S. Cederbaum, "Universal attosecond response to the removal of an electron," *Phys. Rev. Lett.* **94**, 033901 (2005).
4. F. Remacle and R. D. Levine, "An electronic time scale in chemistry," *Proc. Natl. Acad. Sci. U. S. A.* **103**, 6793–6798 (2006).
5. A. I. Kuleff, S. Lünemann, and L. S. Cederbaum, "Electron-correlation-driven charge migration in oligopeptides," *Chem. Phys.* **414**, 100–105 (2013).
6. M. Vacher, M. J. Bearpark, and M. A. Robb, "Communication: oscillating charge migration between lone pairs persists without significant interaction with nuclear motion in the glycine and Gly-Gly-NH-CH<sub>3</sub> radical cations," *J. Chem. Phys.* **140**, 201102 (2014).
7. A. Bruner et al., "Attosecond charge migration with TDDFT: accurate dynamics from a well-defined initial state," *J. Phys. Chem. Lett.* **8**, 3991–3996 (2017).
8. N. V. Golubev and A. I. Kuleff, "Control of charge migration in molecules by ultrashort laser pulses," *Phys. Rev. A* **91**, 051401(R) (2015).
9. V. Despré and A. Kuleff, "Size effects in charge migration in alkyne chains," *Theor. Chem. Accounts* **138**, 110 (2019).
10. A. S. Folorunso et al., "Molecular modes of attosecond charge migration," *Phys. Rev. Lett.* **126**, 133002 (2021).
11. F. Mauger et al., "Charge migration and attosecond solitons in conjugated organic molecules," *Phys. Rev. Res.* **4**, 013073 (2022).
12. F. Mauger et al., "Nonlinear dynamics of attosecond charge migration in model carbon chains," arXiv:2007.08007v1 (2020).
13. W. Yu et al., "Dynamical analysis of attosecond molecular modes," *Phys. Rev. A* **107**, 013101 (2023).
14. M. Vacher et al., "Electron dynamics upon ionization of polyatomic molecules: coupling to quantum nuclear motion and decoherence," *Phys. Rev. Lett.* **118**, 083001 (2017).
15. D. Jia, J. Manz, and Y. Yang, "De- and recoherence of charge migration in ionized iodoacetylene," *J. Phys. Chem. Lett.* **10**, 4273–4277 (2019).
16. V. Despré, N. V. Golubev, and A. I. Kuleff, "Charge migration in propiolic acid: a full quantum dynamical study," *Phys. Rev. Lett.* **121**, 203002 (2018).
17. F. Calegari et al., "Ultrafast electron dynamics in phenylalanine initiated by attosecond pulses," *Science* **346**, 336–339 (2014).
18. F. Calegari et al., "Charge migration induced by attosecond pulses in bio-relevant molecules," *J. Phys. B* **49**, 142001 (2016).
19. M. Lara-Astiaso et al., "Attosecond pump-probe spectroscopy of charge dynamics in tryptophan," *J. Phys. Chem. Lett.* **9**, 4570–4577 (2018).
20. E. P. Månsson et al., "Real-time observation of a correlation-driven sub fs charge migration in ionised adenine," *Comm. Chem.* **4**, 73 (2021).
21. D. T. Matselyukh et al., "Decoherence and revival in attosecond charge migration driven by non-adiabatic dynamics," *Nat. Phys.* **18**, 1206–1213 (2022).
22. S. R. Leone et al., "What will it take to observe processes in 'real time'?" *Nat. Photonics* **8**, 162–166 (2014).

23. F. Lépine, M. Ivanov, and M. Vrakking, “Attosecond molecular dynamics: fact or fiction?” *Nat. Photonics* **8**, 195–204 (2014).
24. P. B. Corkum, “Plasma perspective on strong field multiphoton ionization,” *Phys. Rev. Lett.* **71**, 1994–1997 (1993).
25. M. Lewenstein et al., “Theory of high-harmonic generation by low-frequency laser fields,” *Phys. Rev. A* **49**, 2117–2132 (1994).
26. P. M. Kraus et al., “Measurement and laser control of attosecond charge migration in ionized iodoacetylene,” *Science* **350**, 790–795 (2015).
27. L. He et al., “Filming movies of attosecond charge migration in single molecules with high harmonic spectroscopy,” *Nat. Commun.* **13**, 4595 (2022).
28. Y. Huang et al., “Ultrafast hole deformation revealed by molecular attosecond interferometry,” *Ultrafast Sci.* **2021**, 9837107 (2021).
29. M. Lein, “Attosecond probing of vibrational dynamics with high-harmonic generation,” *Phys. Rev. Lett.* **94**, 053004 (2005).
30. S. Baker et al., “Probing proton dynamics in molecules on an attosecond time scale,” *Science* **312**, 424–427 (2006).
31. P. Lan et al., “Attosecond probing of nuclear dynamics with trajectory-resolved high-harmonic spectroscopy,” *Phys. Rev. Lett.* **119**, 033201 (2017).
32. D. R. Tuthill et al., “Multidimensional molecular high-harmonic spectroscopy: a road map for charge migration studies,” *J. Mol. Spectrosc.* **372**, 111353 (2020).
33. J. Itatani et al., “Tomographic imaging of molecular orbitals,” *Nature* **432**, 867–871 (2004).
34. S. Haessler et al., “Attosecond imaging of molecular electronic wavepackets,” *Nat. Phys.* **6**, 200–206 (2010).
35. C. Vozzi et al., “Generalized molecular orbital tomography,” *Nat. Phys.* **7**, 822–826 (2011).
36. S. Sun et al., “Iterative projection algorithm for retrieval of angle-resolved single-molecule dipoles from high-harmonic spectra,” *Phys. Rev. A* **107**, 033105 (2023).
37. O. Smirnova et al., “High harmonic interferometry of multi-electron dynamics in molecules,” *Nature* **460**, 972–977 (2009).
38. O. Smirnova et al., “Strong-field control and spectroscopy of attosecond electron-hole dynamics in molecules,” *Proc. Natl. Acad. Sci. U. S. A.* **106**, 16556–16561 (2009).
39. Z. Shu et al., “Channel coupling dynamics of deep-lying orbitals in molecular high-harmonic generation,” *Phys. Rev. Lett.* **128**, 183202 (2022).
40. A. T. Le et al., “Quantitative rescattering theory for high-order harmonic generation from molecules,” *Phys. Rev. A* **80**, 013401 (2009).
41. C. D. Lin et al., “Strong-field rescattering physics—self-imaging of a molecule by its own electrons,” *J. Phys. B* **43**, 122001 (2010).
42. C. D. Lin et al., *Attosecond and Strong-Field Physics: Principles and Applications*, Cambridge University Press (2018).
43. C. D. Lin et al., “Elements of the quantitative rescattering theory,” *J. Phys. B* **51**, 104001 (2018).
44. Y. He et al., “Measuring the rotational temperature and pump intensity in molecular alignment experiments via high harmonic generation,” *Opt. Express* **28**, 21182–21191 (2020).
45. K. Yoshii, G. Miyaji, and K. Miyazaki, “Retrieving angular distributions of high-order harmonic generation from a single molecule,” *Phys. Rev. Lett.* **106**, 013904 (2011).
46. L. He et al., “Real-time observation of molecular spinning with angular high-harmonic spectroscopy,” *Phys. Rev. Lett.* **121**, 163201 (2018).
47. Y. He et al., “Direct imaging of molecular rotation with high-order-harmonic generation,” *Phys. Rev. A* **99**, 053419 (2019).
48. H. T. Thai et al., “Evaluation of bootstrap methods for estimating uncertainty of parameters in nonlinear mixed-effects models: a simulation study in population pharmacokinetics,” *J. Pharmacokinet. Pharmacodyn.* **41**, 15–33 (2014).
49. W. Kohn and L. J. Sham, “Self-consistent equations including exchange and correlation effects,” *Phys. Rev.* **140**, A1133–A1138 (1965).
50. E. Runge and E. Gross, “Density-functional theory for time-dependent systems,” *Phys. Rev. Lett.* **52**, 997–1000 (1984).
51. M. Marques et al., “Octopus: a first-principles tool for excited electron-ion dynamics,” *Comput. Phys. Commun.* **151**, 60–78 (2003).
52. J. P. Perdew and A. Zunger, “Self-interaction correction to density-functional approximations for many-electron systems,” *Phys. Rev. B* **23**, 5048–5079 (1981).
53. C. Legrand, E. Suraud, and P. G. Reinhard, “Comparison of self-interaction-corrections for metal clusters,” *J. Phys. B* **35**, 1115 (2002).
54. B. D. Bruner et al., “Multidimensional high harmonic spectroscopy of polyatomic molecules: detecting sub-cycle laser-driven hole dynamics upon ionization in strong mid-IR laser fields,” *Faraday Discuss.* **194**, 369–405 (2016).
55. L. He et al., “Spectrally resolved spatiotemporal features of quantum paths in high-order-harmonic generation,” *Phys. Rev. A* **92**, 043403 (2015).
56. X. M. Tong, Z. X. Zhao, and C. D. Lin, “Theory of molecular tunneling ionization,” *Phys. Rev. A* **66**, 033402 (2002).
57. X. M. Tong and C. D. Lin, “Empirical formula for static field ionization rates of atoms and molecules by lasers in the barrier-suppression regime,” *J. Phys. B* **38**, 2593 (2005).
58. S. Zhao et al., “Determination of structure parameters in strong-field tunneling ionization theory of molecules,” *Phys. Rev. A* **81**, 033423 (2010).

**Lixin He** is an associate professor at Wuhan National Laboratory for Optoelectronics, Huazhong University of Science and Technology (HUST), Wuhan, China. He received his PhD from HUST in 2016. From 2016 to 2018, he worked as a postdoctoral fellow in Prof. Peixiang Lu's group at HUST. His main research interest is high-order harmonic generation and ultrafast imaging of molecular dynamics.

**Yanqing He** received his PhD in ultrafast optics, supervised by Prof. Pengfei Lan, from HUST in 2023. His research focuses on laser-induced molecular alignment and ultrafast molecular imaging.

**Siqi Sun** is a PhD student, supervised by Prof. Pengfei Lan, at HUST. His main research interest is AI algorithms and their applications in ultrafast molecular imaging.

**Esteban Goetz** is a postdoctoral research associate in theoretical atomic physics at the University of Connecticut, USA. He obtained his PhD from Universität Kassel, Germany. He also worked at Kansas State University and Drake University. His research activities and interests include laser-driven ultrafast quantum dynamics and quantum control, with a focus on high-harmonic generation and photoelectron spectroscopy.

**Anh-Thu Le** is a professor at University of Connecticut, USA. He received his PhD from Belarusian State University, Belarus. He also worked at Kansas State University and Missouri University of Science and Technology. His research interests include intense laser-atom/molecule interaction and attosecond physics, with main activities focusing on strong-field ionization, high-harmonic generation spectroscopy, and laser-induced electron diffraction.

**Xiaosong Zhu** is a professor at the School of Physics, HUST, Wuhan, China. He received his PhD from HUST in 2013. From 2018 to 2020, he received the Alexander von Humboldt Research Fellowship and worked at Leibniz Universität Hannover, Germany. His research focuses on high harmonic generation from atoms, molecules, and solids.

**Pengfei Lan** is a professor at the School of Physics, HUST, Wuhan, China. He received his PhD from HUST in 2009. From 2009 to 2013, he worked at RIKEN, Japan. He was selected as a distinguished young scholar of NSFC. His research focuses on the generation of attosecond pulses and high harmonics with atoms, molecules, and solids.

**Peixiang Lu** is a professor and the vice director at Wuhan National Laboratory for Optoelectronics, HUST, Wuhan, China. He received his PhD from Shanghai Institute of Optics and Fine Mechanics. He was selected as a Cheung Kong Scholar Chair Professor and a distinguished

young scholar of NSFC. He was selected as OSA fellow in 2016. His research interest is strong ultrafast optics.

**Chii-Dong Lin** received his PhD in physics in 1974 from the University of Chicago under Prof. Ugo Fano. He has been a professor at Kansas State University since 1976. His research spans many fields of AMO physics. Since 2002, he has contributed several ideas in strong-field physics, including the MO-ADK theory for ionization and the QRS model for electron rescattering and harmonic generation. He also contributed to the characterization of attosecond pulses and dynamics of molecules from intense laser experiments.